

Carbon-Rich Carbon Nitride Monolayers with Dirac Cones: Dumbbell C₄N

Linyang Li^{a,*}, Xiangru Kong^{b,*}, Ortwin Leenaerts^{a,*}, Xin Chen^c, Biplab Sanyal^c, François M. Peeters^{a,*}

^a *Department of Physics, University of Antwerp, Groenenborgerlaan 171, B-2020 Antwerp, Belgium*

^b *International Center for Quantum Materials, Peking University, 100871 Beijing, China*

^c *Department of Physics and Astronomy, Uppsala University, SE-75120 Uppsala, Sweden*

Abstract: Two-dimensional (2D) carbon nitride materials play an important role in energy-harvesting, energy-storage and environmental applications. Recently, a new carbon nitride, 2D polyaniline (C₃N) was proposed [PNAS 113 (2016) 7414-7419]. Based on the structure model of this C₃N monolayer, we propose two new carbon nitride monolayers, named dumbbell (DB) C₄N-I and C₄N-II. Using first-principles calculations, we systematically study the structure, stability, and band structure of these two materials. In contrast to other carbon nitride monolayers, the orbital hybridization of the C/N atoms in the DB C₄N monolayers is sp^3 . Remarkably, the band structures of the two DB C₄N monolayers have a Dirac cone at the K point and their Fermi velocities ($2.6/2.4 \times 10^5$ m/s) are comparable to that of graphene. This makes them promising materials for applications in high-speed electronic devices. Using a tight-binding model, we explain the origin of the Dirac cone.

*Corresponding authors. E-mail addresses:

linyang.li@uantwerpen.be (Linyang Li)

kongxru@pku.edu.cn (Xingru Kong)

ortwin.leenaerts@uantwerpen.be (Ortwin Leenaerts)

francois.peeters@uantwerpen.be (François M. Peeters)

1. Introduction

Monolayer graphene was first realized in 2004 [1] and since then the group IV elemental monolayers have played a crucial role in the field of two-dimensional (2D) materials. In experiments, silicene, germanene, and stanene were all synthesized on different substrates [2-10], such as heterostructures of silicene(germanene)/MoS₂ [6,8] and stanene/Bi₂Se₃ [10], which preserve the hexagonal honeycomb structure of the isolated monolayers. Without spin-orbit coupling (SOC), silicene, germanene, and stanene all have a zero electronic band gap with two bands crossing linearly at the Fermi level and their extremely large Fermi velocity (v_F) makes them ideal materials for high-speed electronic devices [11,12]. Taking SOC into account, they all show a nontrivial band gap at the K point which can reach up to 73.5 meV (stanene), making them promising to realize quantum spin Hall (QSH) effect at room-temperature [12]. Besides the buckled hexagonal honeycomb structure, another stable structure model of Si/Ge/Sn, known as the dumbbell (DB) structure, was proposed in previous studies [13-15]. Different to the band structure of stanene, the DB structure of Sn shows a band inversion at the Γ point due to SOC and was predicted to be a 2D topological insulator [13]. By functionalization, Sn/Ge DB structures show nontrivial band gaps that can reach up to 235 meV [16-19] while the Si DB structure can also become a 2D topological insulator under external strain [20]. In contrast to the extended literature on DB structures of Si/Ge/Sn, studies on the DB structure of C have been scarce up to now [21].

Besides the group IV elemental monolayers and their allotropes, carbon nitride materials are another important set of 2D materials. Many 2D carbon nitride materials can be applied in some important physical and chemical processes. Among these, graphitic carbon nitride (g-C₃N₄) has been studied for a long time [22] and it can be used in many energy applications, such as hydrogen generation

[23], efficient energy storage [24], and photocatalytic degradation of pollutants [25]. Nanoporous carbon nitride materials, such as the C_2N monolayer [26], can be applied in gas separation [27-29] or water desalination [30]. The carbon nitride materials not only have a huge potential in applications but also exhibit many interesting physical effects, including QSH [31], quantum anomalous Hall (QAH) [32,33], and spin-polarization [34,35] effects. More and more new 2D carbon nitride materials have been produced in experiment. Recently, an interesting new 2D carbon nitride material, called polyaniline (C_3N), was synthesized [36]. Its monolayer shows a similar structure as graphene and its band structure is semiconducting with an indirect band gap, in contrast to the Dirac band structure of graphene.

Based on the C_3N monolayer structure and the DB structure of Si/Ge/Sn, we propose two new C_4N monolayers with a DB structure (DB C_4N). According to the positions of the raised C/N atoms, two configurations, DB C_4N -I and DB C_4N -II, can be obtained. Using first-principles calculations, we investigated systematically the structure, energy, stability, and electronic band structure of these two DB C_4N monolayers. Different to other carbon nitride monolayers, all the C and N atoms in the DB C_4N monolayers have sp^3 hybridization. Although the two DB C_4N monolayers have a different structure and ground state energy, the phonon spectra provide convincing evidence for their thermal and dynamical stability. Similar to the Dirac cone band structure of graphene, the two DB C_4N monolayers both show a Dirac cone at the K point with a large Fermi velocity. An analysis of the projected electron density of states (PDOS) and the electron wave functions of the Dirac cones shows that four p_z atomic orbitals are responsible for the Dirac cone in these two C_4N monolayers. This is also supported by our tight-binding (TB) model including four p_z atomic orbitals that reproduces the first-principles results quite well.

2. Calculation Method

Our first-principles calculations were performed using the Vienna *ab initio* simulation package (VASP) code [37-39], implementing density functional theory (DFT). The electron exchange-correlation functional was treated using the generalized gradient approximation (GGA) in the form proposed by Perdew, Burke, and Ernzerhof (PBE) [40]. The atomic positions and lattice vectors were fully optimized using the conjugate gradient (CG) scheme until the maximum force on each atom was less than 0.01 eV/Å. The energy cutoff of the plane-wave basis was set to 520 eV with an energy precision of 10^{-5} eV. The Brillouin zone (BZ) was sampled by using a $17 \times 17 \times 1$ Γ -centered Monkhorst-Pack grid. The vacuum space was set to at least 20 Å in all the calculations to minimize artificial interactions between neighboring slabs. The phonon spectra were calculated using a supercell approach within the PHONOPY code [41].

3. Results and Discussions

3.1 Geometrical Structure

The two investigated DB C₄N monolayers are shown in Figure 1(a) and (b). They are based on the C₃N monolayer (Figure 1(c)), which was recently synthesized in experiment [36]. By adsorbing C atoms on all the N atom positions of the C₃N monolayer, we obtain two different DB C₄N monolayers. The two patterns are classified as follows: (1) If the raised N/C atoms are on one side of the monolayer, as shown in Figure 1(a), we call it DB C₄N-I; (2) If the raised N/C atoms are on two opposite sides of the monolayer, as shown in Figure 1(b), we call it DB C₄N-II. In the following, we will analyze the three monolayers (DB C₄N-I, DB C₄N-II, and C₃N) from the points of view of symmetry, orbital hybridization style, and bond length.

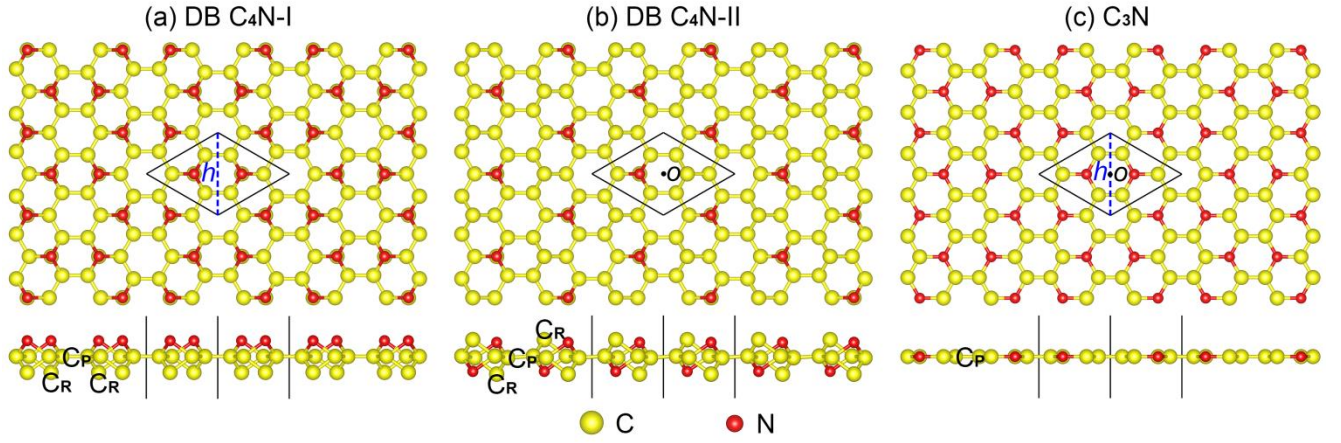


Figure 1. Schematic representations (top and side views) of the DB C₄N-I (a), DB C₄N-II (b) and C₃N (c). The raised C atoms are labeled as C_R and the planar C atoms are labeled as C_P. The yellow (red) symbols are the carbon (nitrogen) atoms.

Considering symmetry first, the C₃N monolayer has higher symmetry than the C₄N monolayers. For the C₃N monolayer, the C/N atoms are not only center symmetric about the point *o* (black point, Figure 1(c)), but also mirror symmetric about the plane *h* (blue dashed line, Figure 1(c)) parallel to the *z* axis. However, the C/N atoms of the DB C₄N-I are only mirror symmetric about the plane *h* (blue dashed line, Figure 1(a)) parallel to the *z* axis while the C/N atoms of the DB C₄N-II are only center symmetric about the point *o* (black point, Figure 1(b)). Next, let us take a look at the hybridization of the atoms. The C/N atoms in the C₃N monolayer have sp^2 hybridization, similar to the atoms in graphene or g-C₃N₄. On the other hand, all the C/N atoms in the DB C₄N monolayers have sp^3 hybridization, similar to the C atoms in diamond.

Corresponding to the change in hybridization, their bond lengths are very different. There are three kinds of atoms in the DB C₄N monolayers, N atoms, raised C (C_R) atoms, and planar C (C_P) atoms, while there are only N atoms and C_P atoms in the C₃N monolayer. In the following, we will discuss the

bonds between the different atoms. Considering the N-C_P bond, one N atom can form a bond with three C_P atoms and the lengths of the three bonds are the same, labeled as L . For the DB C₄N-I and C₄N-II, $L = 1.558$ Å and $L = 1.545$ Å, respectively, which is larger than the $L = 1.403$ Å in C₃N. Between the C atoms, only C_P-C_P bonds are found in the C₃N monolayer and we label them as M ($M = 1.404$ Å). Similar bonds are also found in the DB C₄N monolayers. The C_P atoms of the DB C₄N-I are all in the same xy plane. However, there is a little buckling (0.095 Å) along the z axis between the C_P atoms in the DB C₄N-II due to the inequivalence of the N and C_R atoms. The M of the DB C₄N-I and C₄N-II is 1.491 Å and 1.488 Å, respectively. There is also another C-C bond in the DB C₄N monolayers between the C_R atom and the C_P atom, which is labeled as M' . The M' of the DB C₄N-I (C₄N-II) is 1.567 Å (1.583 Å). From the above data of bond lengths, we can summarize that all the bond lengths in the two DB C₄N monolayers are 1.49~1.58 Å, which is much larger than the 1.40 Å in the C₃N monolayer. A similar difference is also found in the C-C bond length of diamond (1.54 Å) [42] and graphene (1.42 Å) [43], which comes from the different hybridization of the C atoms (sp^3 and sp^2). In most experimental and predicted carbon nitride monolayers, the C and N atoms have sp^2/sp hybridization, while the carbon nitride monolayers with sp^3 -hybridized C/N atoms are rarely studied [44]. Here, we provide a novel structure model for new stable carbon nitride monolayers. Although there is much difference in bond length, the lattice constants of the C₃N (4.861 Å) and the DB C₄N (4.775 Å (C₄N-I) and 4.768 Å (C₄N-II)) are almost the same. The optimized geometrical structure data are summarized in Table 1.

Table 1. Structure parameters and formation energies of the DB C₄N and C₃N monolayers. a is the lattice constant. L , M , and M' are the lengths of the N-C_P, C_P-C_P, and C_P-C_R bonds, respectively. The

unit of a , L , M , and M' is Å. The formation energy ΔE corresponds to the energy release of the C_3N monolayer adsorbing isolated magnetic C atoms (eV/C atom).

	a	$L(N-C_P)$	$M(C_P-C_P)$	$M'(C_P-C_R)$	ΔE
C_4N-I	4.775	1.558	1.491	1.567	-3.272
C_4N-II	4.768	1.545	1.488	1.583	-3.379
C_3N	4.861	1.403	1.404	--	--

3.2 Energy and Stability

We calculated the formation energies of the DB C_4N monolayers as the difference in energy between the DB C_4N and the sum of the energies of the C_3N monolayer and isolated magnetic C atoms [45]. The formation energy ΔE of the DB C_4N-I (C_4N-II) is -3.272 eV/C atom (-3.379 eV/C atom), which is of the same magnitude as adsorbed C atoms on graphene [46]. The negative formation energy suggests the stability and feasibility of the DB C_4N . In experiment, carbon atoms and carbon atomic chains have been observed on graphene using transmission electron microscope (TEM) and TEM studies demonstrated that individual carbon atoms can be adsorbed on graphene surfaces with a stable structure at room-temperature [47-48]. Since 2D C_3N has been realized in experiment, the DB C_4N monolayers are probably also suited for experimental synthesis.

Considering the two DB C_4N monolayers, the energy of the DB C_4N-II is lower than that of the DB C_4N-I . This can be ascribed to the differences in their structures. The DB C_4N-I monolayer exhibits a polarized structure due to the absence of inversion symmetry while the DB C_4N-II has no dipole moment. From the views of energy and symmetry, the DB C_4N-II is more stable than the DB C_4N-I . Although the two DB C_4N monolayers have different ground state energies, their phonon spectra (shown in Figure 2)

are both free from imaginary frequency modes, which indicates that they are dynamically stable.

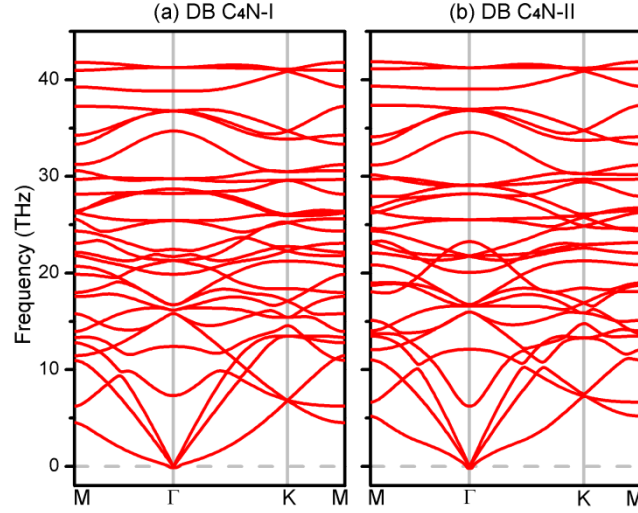


Figure 2. Phonon spectra of DB C₄N-I (a) and DB C₄N-II (b) along the high-symmetry lines in the BZ.

3.3 Band Structure

The electronic band structure of the DB C₄N-I and C₄N-II monolayers is shown in Figure 3. For both cases, a zero band gap at the K point is seen. Two bands cross linearly at the Fermi level and the charge carriers can be characterized by massless Dirac fermions, similar to the band structure of graphene (silicene/germanene/stanene) at the K point [11,12]. By a linear fitting of the first-principles data, we can obtain the Fermi velocity of the DB C₄N. For the DB C₄N-I (C₄N-II), the Fermi velocity is 2.6×10^5 m/s (2.4×10^5 m/s), which is comparable to that of the group IV elemental monolayers ($4.70 \sim 8.46 \times 10^5$ m/s) [12]. The extremely large Fermi velocity makes the DB C₄N monolayers ideal materials for building high-speed electronic devices, such as field effect transistors (FET). It is well known that there are many kinds of Dirac carbon monolayers in experiment and theory, such as graphene [1], $\alpha/\beta/\delta/6,6,12$ -graphyne [49-51], phagraphene [52], etc. However, the 2D carbon nitride

materials in experiment, such as g-C₃N₄, C₂N, and g-C₆N₆ monolayers, all show semiconductor behavior with a band gap of 2.73 eV [53], 1.96 eV [26], and 1.53 eV [31], respectively. Dirac cone band structures for carbon nitride materials are rarely predicted and only the g-C₁₄N₁₂ and g-C₁₀N₉ were proposed as spin-polarized Dirac materials [32,33]. To our knowledge, the two DB C₄N monolayers are the first predicted Dirac carbon nitride materials without spin-polarization. In contrast to the g-C₆N₆ monolayer proposed by Wang *et al.* [31], the Dirac cone of the DB C₄N is right at the Fermi level, which is advantageous for experiments and applications.

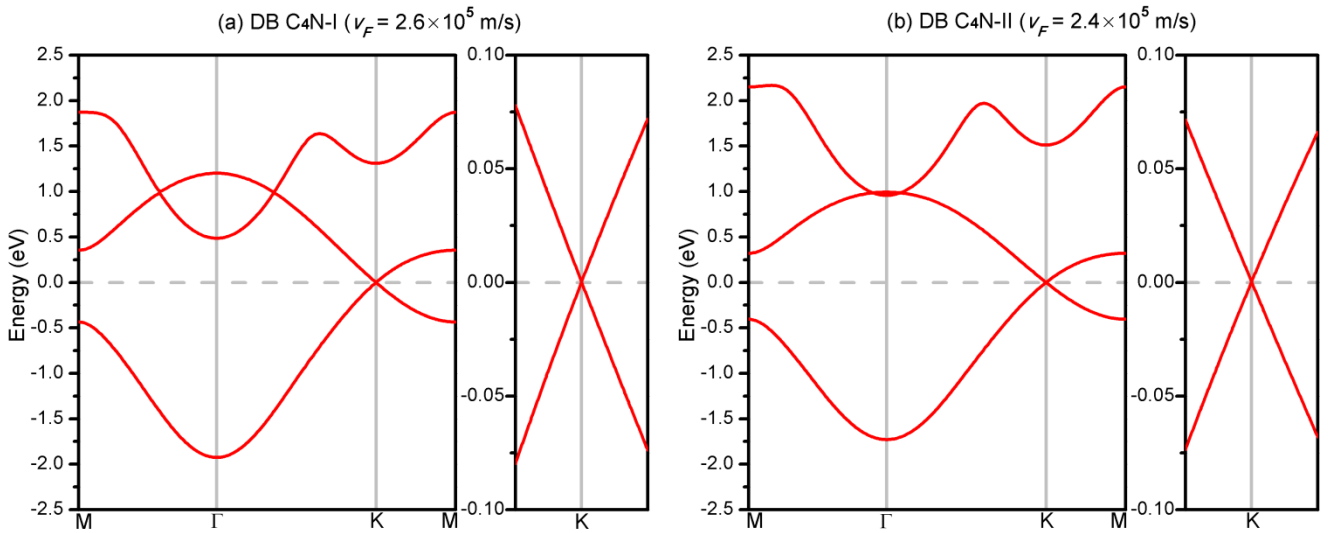


Figure 3. Band structure of DB C₄N-I (a) and DB C₄N-II (b) monolayers from DFT calculations. v_F is the Fermi velocity of the Dirac cone. The energy at the Fermi level was set to zero. An enlarged view of the band lines at the K point near the Fermi level is presented on the right.

To investigate the origin of the Dirac cones, we calculated the PDOS for different atomic orbitals and the Kohn-Sham wave functions at the Dirac points, as shown in Figure 4. From the PDOS analysis

of the two DB C₄N monolayers, it is clear that the summed states of the s , p_x , and p_y atomic orbitals around the Fermi level are far less than the PDOS corresponding to the p_z atomic orbitals. Although the C/N atoms are sp^3 -hybridized ($(sp^3)_z = 1/2s + \sqrt{3}/2p_z$), the states close to the Fermi level mainly come from the p_z atomic orbitals, which is similar to graphene/graphyne [49-52]. As for phagraphene where only the p_z orbitals of eight out of twenty C atoms in the unit cell are responsible for the formation of the Dirac cone [54], not all ten atoms in the unit cell of the DB C₄N contribute to the Dirac cone. Only the two C_R and the two N atoms play an important role in the formation of the Dirac cone, which is clearly shown in the corresponding Kohn-Sham wave functions at the Dirac point (Figure 4(a) and (b)).

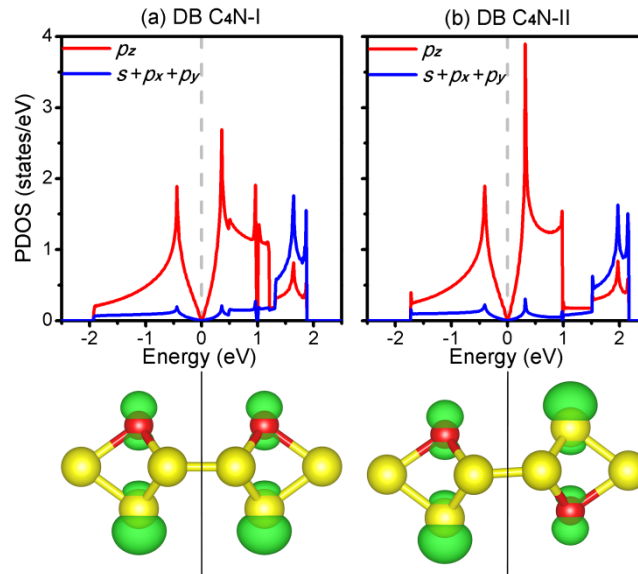


Figure 4. The PDOS for the summed states of the s , p_x , and p_y/p_z atomic orbitals of all the atoms in the unit cell and the corresponding Kohn-Sham wave functions at the Dirac points. The isosurface values of the Kohn-Sham wave functions were set to 0.02 \AA^{-3} .

We also investigated the SOC effect on the band structures of the DB C₄N monolayers. For the DB

C₄N monolayers, the SOC effect is very small with the value of the band gap at the K point below 0.25 meV. This will be difficult to be detected in a real experiment because of the possible presence of disorder. We can understand the weak SOC effect from two aspects. First, the SOC effect is related to the element type: the heavier the element, the more pronounced the SOC effect becomes. Structures including heavy elements, such as Bi, can have a large SOC effect [55, 56]. Second, the SOC effect is also related to the atomic orbitals forming the Dirac cone. For the g-C₆N₆ monolayer, the SOC band gap of the Dirac cone at the K point (below the Fermi level) can reach 5.50 meV [31]. In this case the Dirac cone is formed by the p_x and p_y atomic orbitals of the N atoms and the SOC gap originates directly from the onsite term. According to the PDOS and the corresponding Kohn-Sham wave functions of the Dirac point, the four p_z atomic orbitals of the C_R and N atoms in the DB C₄N are responsible for the formation of the Dirac cone, which is the main reason for the weak SOC effect. The band gap values of the DB C₄N monolayers are between the 0.008 meV of graphene and the 0.59 meV of δ -graphyne [51], where the Dirac cones are formed by the p_z atomic orbitals of the C atoms.

3.4 TB model

Although the two C_R and the two N atoms all contribute to the Dirac cone, it is clear that the Kohn-Sham wave functions of the C_R atoms are much larger than those of the N atoms for both DB C₄N monolayers (Figure 4). We can understand the origin of the Dirac cone from a simple TB model by only including the p_z atomic orbitals of the two C_R atoms without the two N atoms. The two DB C₄N monolayers can be regarded as to consist of two C_R atoms in one unit cell. Setting \vec{a}_1 and \vec{a}_2 as the primitive vectors, the positions of the two C_R atoms in the xy plane can be expressed as $1/3 \times (\vec{a}_1 + \vec{a}_2)$ and

$2/3 \times (\vec{a}_1 + \vec{a}_2)$, similar to graphene/silicene. The DB C₄N-I can be regarded as a structure of graphene because the two C_R atoms are in the same xy plane while the DB C₄N-II can be regarded as a structure of silicene due to the buckling along the z axis between the two C_R atoms. The two C_R atoms in the unit cell can be labeled as A and B atoms. The TB Hamiltonian that describes the electronic structure near the Fermi level of such a system can be written as [57,58]

$$H = \begin{pmatrix} \varepsilon & \hbar v_F (k_x - i k_y) \\ \hbar v_F (k_x + i k_y) & -\varepsilon \end{pmatrix},$$

where k is the wave vector relative to the Dirac point and v_F is the Fermi velocity. Similar to graphene/silicene, the difference of the onsite energy between the two C_R atoms is zero because they have the same chemical environment [59,60]. Thus we obtain a linear dispersion relation $E = \pm \hbar v_F |k|$, which is the origin of the Dirac cone.

Although the above simple model leads to a direct understanding of the Dirac cone, the two N atoms still have contributions in the formation of the Dirac cone. We further confirm these results by a TB model including the p_z atomic orbitals of the two C_R and two N atoms in the unit cell [54]. We resorted to maximally localized Wannier functions (MLWFs) [61] using the Wannier90 code [62]. Starting from the bands of the first-principles calculations, we used the four p_z atomic orbitals of the C_R and N atoms. Minimizing the MLWF spread, the band structures obtained using the Wannier90 interpolation method and the DFT calculations are in excellent agreement, as shown in Figure 5.

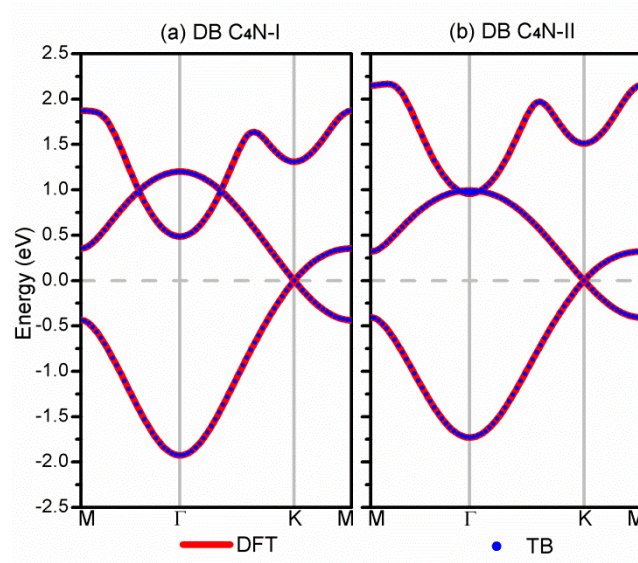


Figure 5. Band structure of DB C₄N-I (a) and DB C₄N-II (b) from DFT and TB calculations. The red lines represent the results of DFT calculations and the blue dotted lines represent the results of TB calculations.

4. Conclusion

In summary, using first-principles calculations, we predict the first Dirac carbon nitride monolayers without spin-polarization. In contrast to the existing 2D carbon nitride materials that have been realized in experiments, they have a dumbbell structure and all the C and N atoms are sp^3 -hybridized. Their formation energies compared to C₃N and phonon calculations fully confirm their energetic and dynamical stability. The Dirac cone band structure and large Fermi velocity are comparable to graphene and make the DB C₄N monolayers promising materials for high-speed electronic devices. A simple TB model was constructed in order to understand the origin of the Dirac cone which is helpful for further investigations of the massless Dirac fermions. The here proposed DB C₄N monolayer structures provide a new way to search for Dirac cone band structures in group IV-V elemental materials.

Acknowledgements

This work was supported by the Fonds Wetenschappelijk Onderzoek (FWO-VI). The computational resources and services used in this work were provided by the VSC (Flemish Supercomputer Center), funded by the Research Foundation - Flanders (FWO) and the Flemish Government – department EWI. X. C. acknowledges financial support from the China Scholarship Council (CSC).

References

- [1] K. S. Novoselov, A. K. Geim, S. V. Morozov, D. Jiang, Y. Zhang, S. V. Dubonos, et al., Electric Field Effect in Atomically Thin Carbon Films, *Science* 306 (2004) 666-669.
- [2] B. Feng, Z. Ding, S. Meng, Y. Yao, X. He, P. Cheng, et al., Evidence of Silicene in Honeycomb Structures of Silicon on Ag(111), *Nano Lett.* 12 (2012) 3507-3511.
- [3] P. Vogt, P. De Padova, C. Quaresima, J. Avila, E. Frantzeskakis, M. C. Asensio, et al., Silicene: Compelling Experimental Evidence for Graphenelike Two-dimensional Silicon, *Phys. Rev. Lett.* 108 (2012) 155501.
- [4] D. Chiappe, C. Grazianetti, G. Tallarida, M. Fanciulli, A. Molle, Local Electronic Properties of Corrugated Silicene Phases, *Adv. Mater.* 24 (2012) 5088-5093.
- [5] L. Meng, Y. Wang, L. Zhang, S. Du, R. Wu, L. Li, et al., Buckled Silicene Formation on Ir(111), *Nano Lett.* 13 (2013) 685-690.
- [6] D. Chiappe, E. Scalise, E. Cinquanta, C. Grazianetti, B. van den Broek, M. Fanciulli, et al., Two-dimensional Si Nanosheets with Local Hexagonal Structure on a MoS₂ Surface, *Adv. Mater.* 26 (2014) 2096-2101.
- [7] M. Derivaz, D. Dentel, R. Stephan, M. C. Hanf, A. Mehdaoui, P. Sonnet, et al., Continuous Germanene Layer on Al(111), *Nano Lett.* 15 (2015) 2510-2516.
- [8] L. Zhang, P. Bampoulis, A. N. Rudenko, Q. Yao, A. van Houselt, B. Poelsema, et al., Structural and Electronic Properties of Germanene on MoS₂, *Phys. Rev. Lett.* 116 (2016) 256804.
- [9] J. Gou, Q. Zhong, S. Sheng, W. Li, P. Cheng, H. Li, et al., Strained monolayer germanene with 1×1 lattice on Sb(111), *2D Mater.* 3 (2016) 045005.

- [10] F. F. Zhu, W. J. Chen, Y. Xu, C. L. Gao, D. D. Guan, C. H. Liu, et al., Epitaxial growth of two-dimensional stanene, *Nature Mater.* 14 (2015) 1020-1025.
- [11] C. C. Liu, W. Feng, Y. Yao, Quantum Spin Hall Effect in Silicene and Two-Dimensional Germanium, *Phys. Rev. Lett.* 107 (2011) 076802.
- [12] C. C. Liu, H. Jiang, Y. Yao, Low-energy effective Hamiltonian involving spin-orbit coupling in silicene and two-dimensional germanium and tin, *Phys. Rev. B* 84 (2011) 195430.
- [13] P. Tang, P. Chen, W. Cao, H. Huang, S. Cahangirov, L. Xian, et al., Stable two-dimensional dumbbell stanene: A quantum spin Hall insulator, *Phys. Rev. B* 90 (2014) 121408(R).
- [14] V. Ongun Özçelik, S. Ciraci, Local Reconstructions of Silicene Induced by Adatoms, *J. Phys. Chem. C* 117 (2013) 26305-26315.
- [15] V. Ongun Özçelik, E. Durgun, S. Ciraci, New Phases of Germanene, *J. Phys. Chem. Lett.* 5 (2014) 2694-2699.
- [16] X. Chen, L. Li, M. Zhao, Dumbbell stanane: a large-gap quantum spin hall insulator, *Phys. Chem. Chem. Phys.* 17 (2015) 16624-16629.
- [17] X. Chen, L. Li, M. Zhao, Hydrogenation-induced large-gap quantum-spin-Hall insulator states in a germanium–tin dumbbell structure, *RSC Adv.* 5 (2015) 72462-72468.
- [18] H. Zhang, J. Zhang, B. Zhao, T. Zhou, Z. Yang, Quantum anomalous Hall effect in stable dumbbell stanene, *Appl. Phys. Lett.* 108 (2016) 082104.
- [19] Y. P. Wang, W. X. Ji, C. W. Zhang, P. Li, F. Li, P. J. Wang, et al., Large-gap quantum spin Hall state in functionalized dumbbell stanene, *Appl. Phys. Lett.* 108 (2016) 073104.
- [20] T. Zhang, Z. Y. Zeng, Y. Cheng, X. R. Chen, L. C. Cai, Dumbbell silicene: a strain-induced room

temperature quantum spin Hall insulator, New J. Phys. 18 (2016) 043001.

[21] V. Ongun Özçelik, D. Kecik, E. Durgun, S. Ciraci, Adsorption of Group IV Elements on Graphene, Silicene, Germanene, and Stanene: Dumbbell Formation, J. Phys. Chem. C 119 (2015) 845-853.

[22] E. C. FRANKLIN, THE AMMONO CARBONIC ACIDS, J. Am. Chem. Soc. 44 (1922) 486-509.

[23] S. Cao, J. Yu, g-C₃N₄-Based Photocatalysts for Hydrogen Generation, J. Phys. Chem. Lett. 5 (2014) 2101-2107.

[24] M. Wu, Q. Wang, Q. Sun, P. Jena, Functionalized Graphitic Carbon Nitride for Efficient Energy Storage, J. Phys. Chem. C 117 (2013) 6055-6059.

[25] Z. Zhao, Y. Sun, F. Dong, Graphitic carbon nitride based nanocomposites: a review, Nanoscale 7 (2015) 15-37.

[26] J. Mahmood, E. K. Lee, M. Jung, D. Shin, I. Y. Jeon, S. M. Jung, et al., Nitrogenated holey two-dimensional structures, Nat. Commun. 6 (2015) 6486.

[27] B. Xu, H. Xiang, Q. Wei, J. Q. Liu, Y. D. Xia, J. Yin, et al., Two-dimensional graphene-like C₂N: an experimentally available porous membrane for hydrogen purification, Phys. Chem. Chem. Phys. 17 (2015) 15115-15118.

[28] Y. Qu, F. Li, H. Zhou, M. Zhao, Highly Efficient Quantum Sieving in Porous Graphene-like Carbon Nitride for Light Isotopes Separation, Sci. Rep. 6 (2016) 19952.

[29] F. Li, Y. Qu, M. Zhao, Efficient helium separation of graphitic carbon nitride membrane, Carbon 95 (2015) 51-57.

[30] Y. Yang, W. Li, H. Zhou, X. Zhang, M. Zhao, Tunable C₂N Membrane for High Efficient Water Desalination, Sci. Rep. 6 (2016) 29218.

- [31] A. Wang, X. Zhang, M. Zhao, Topological insulator states in a honeycomb lattice of s-triazines, *Nanoscale* 6 (2014) 11157-11162.
- [32] X. Zhang, A. Wang, M. Zhao, Spin-gapless semiconducting graphitic carbon nitrides: A theoretical design from first principles, *Carbon* 84 (2015) 1-8.
- [33] X. Zhang, M. Zhao, Prediction of quantum anomalous Hall effect on graphene nanomesh, *RSC Adv.* 5 (2015) 9875-9880.
- [34] X. Zhang, M. Zhao, A. Wang, X. Wang, A. Du, Spin-polarization and ferromagnetism of graphitic carbon nitride materials, *J Mater. Chem. C* 1 (2013) 6265-6270.
- [35] A. Du, S. Sanvito, S. C. Smith, First-principles Prediction of Metal-Free Magnetism and Intrinsic Half-Metallicity in Graphitic Carbon Nitride, *Phys. Rev. Lett.* 108 (2012) 197207.
- [36] J. Mahmood, E. K. Lee, M. Jung, D. Shin, H. J. Choi, J. M. Seo, et al., Two-dimensional polyaniline (C_3N) from carbonized organic single crystals in solid state, *PNAS* 113 (2016) 7414-7419.
- [37] G. Kresse, J. Furthmüller, Efficient iterative schemes for *ab initio* total-energy calculations using a plane-wave basis set, *Phys. Rev. B* 54 (1996) 11169-11186.
- [38] G. Kresse, D. Joubert, From ultrasoft pseudopotentials to the projector augmented-wave method, *Phys. Rev. B* 59 (1999) 1758-1775.
- [39] G. Kresse, J. Hafner, *Ab initio* molecular dynamics for open-shell transition metals, *Phys. Rev. B* 48 (1993) 13115-13118.
- [40] J. P. Perdew, K. Burke, M. Ernzerhof, Generalized Gradient Approximation Made Simple, *Phys. Rev. Lett.* 77 (1996) 3865-3868.
- [41] A. Togo, I. Tanaka, First principles phonon calculations in materials science, *Scripta Mater.* 108

(2015) 1-5.

[42] T. HOM, W. KISZENICK, B. POST, Accurate Lattice Constants from Multiple Reflection Measurements II. Lattice Constants of Germanium, Silicon and Diamond, *J. Appl. Cryst.* 8 (1975) 457-458.

[43] X. Zhao, L. Li, M. Zhao, Lattice match and lattice mismatch models of graphene on hexagonal boron nitride from first principles, *J. Phys.: Condens. Matter* 26 (2014) 095002.

[44] S. Zhang, J. Zhou, Q. Wang, P. Jena, Beyond Graphitic Carbon Nitride: Nitrogen-Rich Penta-CN₂ Sheet, *J. Phys. Chem. C* 120 (2016) 3993-3998.

[45] B. Yang, H. Zhou, X. Zhang, M. Zhao, Electron spin-polarization and band gap engineering in carbon-modified graphitic carbon nitrides, *J. Mater. Chem. C* 3 (2015) 10886-10891.

[46] C. Ataca, E. Aktürk, H. Şahin, S. Ciraci, Adsorption of carbon adatoms to graphene and its nanoribbons, *J. Appl. Phys.* 109 (2011) 013704.

[47] J. C. Meyer, C. O. Girit, M. F. Crommie, A. Zettl, Imaging and dynamics of light atoms and molecules on graphene, *Nature (London)* 454 (2008) 319-322.

[48] U. Bangert, M. H. Gass, A. L. Bleloch, R. R. Nair, J. Eccles, Nanotopography of graphene, *Phys. Status Solidi A* 206 (2009) 2115-2119.

[49] D. Malko, C. Neiss, F. Viñes, A. Görling, Competition for Graphene: Graphynes with Direction-Dependent Dirac Cones, *Phys. Rev. Lett.* 108 (2012) 086804.

[50] A. Wang, L. Li, X. Wang, H. Bu, M. Zhao, Graphyne-based carbon allotropes with tunable properties: From Dirac fermion to semiconductor, *Diamond Relat. Mater.* 41 (2014) 65-72.

[51] M. Zhao, W. Dong, A. Wang, Two-dimensional carbon topological insulators superior to graphene,

Sci. Rep. 3 (2013) 3532.

[52] Z. Wang, X. F. Zhou, X. Zhang, Q. Zhu, H. Dong, M. Zhao, et al., Phagraphene: A Low-Energy Graphene Allotrope Composed of 5-6-7 Carbon Rings with Distorted Dirac Cones, Nano Lett. 15 (2015) 6182-6186.

[53] A. Du, S. Sanvito, Z. Li, D. Wang, Y. Jiao, T. Liao, et al., Hybrid Graphene and Graphitic Carbon Nitride Nanocomposite: Gap Opening, Electron–Hole Puddle, Interfacial Charge Transfer, and Enhanced Visible Light Response, J. Am. Chem. Soc. 134 (2012) 4393-4397.

[54] A. Lopez-Bezanilla, Strain-Mediated Modification of Phagraphene Dirac Cones, J. Phys. Chem. C 120 (2016) 17101-17105.

[55] L. Li, X. Zhang, X. Chen, M. Zhao, Giant Topological Nontrivial Band Gaps in Chloridized Gallium Bismuthide, Nano Lett. 15 (2015) 1296-1301.

[56] L. Li, O. Leenaerts, X. Kong, X. Chen, M. Zhao, F. M. Peeters, Gallium Bismuth Halides GaBi-X₂ (X= I, Br, Cl) Monolayers with Distorted Hexagonal Framework: Novel Room-Temperature Quantum Spin Hall Insulators, arXiv:1609.06790 [cond-mat.mtrl-sci] (2016).

[57] L. Li, M. Zhao, Structures, Energetics, and Electronic Properties of Multifarious Stacking Patterns for High-Buckled and Low-Buckled Silicene on the MoS₂ Substrate, J. Phys. Chem. C 118 (2014) 19129-19138.

[58] J. B. OOSTINGA, H. B. HEERSCHE, X. LIU, A. F. MORPURGO, L. M. K. VANDERSYPEN, Gate-induced insulating state in bilayer graphene devices, Nature Mater. 7 (2007) 151-157.

[59] L. Li, X. Wang, X. Zhao, M. Zhao, Moiré superstructures of silicene on hexagonal boron nitride: A first-principles study, Phys. Lett. A 377 (2013) 2628-2632.

- [60] L. Li, M. Zhao, First-principles identifications of superstructures of germanene on Ag(111) surface and h-BN substrate, *Phys. Chem. Chem. Phys.* 15 (2013) 16853-16863.
- [61] N. Marzari, D. Vanderbilt, Maximally localized generalized Wannier functions for composite energy bands, *Phys. Rev. B* 56 (1997) 12847-12865.
- [62] A. A. Mostofi, J. R. Yates, Y. S. Lee, I. Souza, D. Vanderbilt, N. Marzari, wannier90: A tool for obtaining maximally-localised Wannier functions, *Comput. Phys. Commun.* 178 (2008) 685-699.